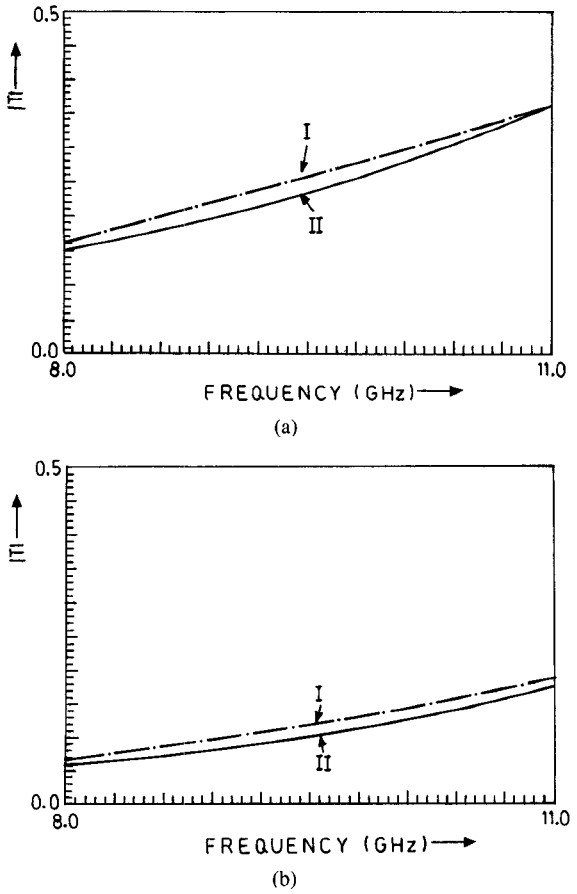

Fig. 3. Variation of the magnitude of transmission coefficient of a single thick aperture in a rectangular waveguide with frequency. (a) For aperture thickness of 0.32 cm. i → Present method. ii → Experimental curve. (b) Same curves for aperture thickness of 0.638 cm.

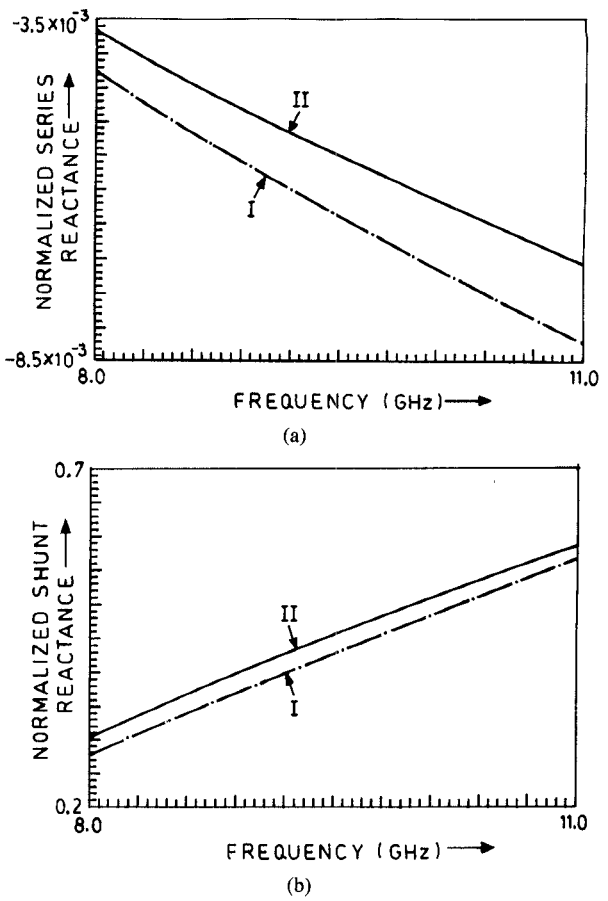

Fig. 4. Variation of the normalized equivalent circuit elements for a centered post of rectangular cross-section with frequency. (a) Plot of normalized series element z_1. i → Present method. ii → Result obtained using Marcuvitz's formula. (b) Same curve for normalized shunt element z_2.

the formulation suggested by Marcuvitz shows a considerable deviation which increases with increasing frequency. The same trend is also observed for the equivalent network parameters presented in Fig. 4(a) and (b). It is therefore concluded that the moment method formulation used in the present work yields more accurate results as compared to the variational formulation. This may be ascribed to the inclusion of the effect of the higher order modes in the stub waveguide which the variational method does not permit. It is worthwhile to pointout that the moment method formulation used in the present paper takes into account the mutual interactions between the interfaces I and II as well as III and IV. The method can also be extended to the case of multiple apertures.

References

[1] N. Marcuvitz, *Waveguide Handbook*. New York: Dover, 1965.
[2] R. E. Collin, *Field Theory of Guided Waves*. New York: McGraw-Hill, 1960.
[3] R. W. Scharstein and A. T. Adams, "Galerkins solution for the thin circular iris in a TE_{11}-mode circular waveguide," *IEEE Trans. Microwave Theory Tech.*, vol. 36, pp. 106–113, 1988.
[4] H. Auda and R. F. Harrington, "Inductive posts and diaphragms of arbitrary shape and number in a rectangular waveguide," *IEEE Trans. Microwave Theory Tech.*, vol. MTT-32, pp. 606–613, 1984.
[5] B. N. Das, P. V. D. S. Rao, and A. Chakraborty, "Narrow wall axial-slot-coupled T junction between rectangular and circular waveguide," *IEEE Trans. Microwave Theory Tech.*, vol. 37, pp. 1590–1596, 1989.
[6] R. F. Harrington, *Time-Harmonic Electromagnetic Fields*. New York: McGraw-Hill, 1961.
[7] R. E. Collin, *Foundations for Microwave Engineering*. Tokyo: McGraw-Hill Kogakusha Ltd., 1966.

Complex Images of an Electric Dipole in Homogeneous and Layered Dielectrics Between Two Ground Planes

J. J. Yang, Y. L. Chow, G. E. Howard, and D. G. Fang

***Abstract*—In this paper, simple closed form expressions are derived for the vector and scalar potentials of a horizontal electric dipole in**

Manuscript received June 4, 1991; revised October 4, 1991. This work was supported by the Communications Research Center, Canada, through contract 3600001-9-3581/01-55, and the Natural Science Foundation of China.

J. J. Yang, Y. L. Chow, and G. E. Howard are with the Department of Electrical and Computer Engineering, University of Waterloo, Waterloo, ON, Canada N2L 3GL.

D. G. Fang is with the East China Institute of Technology, Nanjing, China 210014.

IEEE Log Number 9105439.

homogeneous and layered dielectrics between two ground planes. For the homogeneous dielectric case, an infinite number of dipole images due to the top and bottom ground planes are replaced by a few complex dipole images. For the layered dielectric case, the dipole images due to both the dielectric interfaces and the ground planes are replaced by a few complex dipole images. In addition, the waveguide modes of LSE and LSM types trapped by the two ground planes, and the surface wave modes of LSE and LSM types trapped by the dielectric slabs, both excited by the dipole, are included in the closed form expressions. The accuracy of the closed form expressions is confirmed by the numerical integration of spectral integrals.

I. Introduction

The vector and scalar potentials of a horizontal and infinitesimal electric dipole in a homogeneous dielectric bounded by two ground planes, as shown in Fig. 1(a), can be expressed in either an infinite image expansion or an infinite modal expansion [2]. It has been shown in [3] that the image expansion converges very slowly when the observation point is far (e.g., $>0.2\lambda_0$) from the dipole, and the modal expansion converges very slowly when the observation point is close (e.g., $<0.02\lambda_0$) to the dipole. As a consequence, a "relay race" scheme of image and modal expansions was used in calculating the vector and scalar potential Green's functions in the analysis of complex stripline circuits [3]. A similar scheme was also used in a static analysis of two dimensional homogeneous striplines with finite metallization thickness [4].

For an electric dipole in a layered dielectric between two ground planes, e.g., a microstrip substrate shielded by a grounded top plate (Fig. 1(b)), the vector and scalar potential Green's functions are usually represented as spectral integrals, from which a modal expansion can in principle be obtained. The spectral function of a dipole in general multilayer dielectric substrates has been discussed in [5]. Due to the presence of dielectric interfaces, all the wavenumbers appearing in the modal expansion have to be found numerically by solving the eigenvalue equations of the LSE and LSM modes. This modal expansion will be slowly convergent when the observation point is close to the dipole.

In this paper, we use the complex image technique of [1] to derive simple closed form expressions of the vector and scalar potentials for the problems shown in Fig. 1(a)-(b). Compared to the open microstrip substrate of [1], two new issues arise due to the presence of the two ground planes. The first one is that the summation of the quasi-dynamic images obtained under the approximate condition $k_{z0} \approx k_{z1}$ in spectral integrals [1], [6] converges very slowly when the observation point is far from the dipole. This implies that extracting quasi-dynamic images is not efficient when two ground planes exist. The second issue is that the waveguide modes of LSE and LSM types can exist between the two ground planes. These waveguide modes must be extracted from the spectral integrals, along with the surface wave modes supported by the dielectric slabs. These two problems will be solved in this paper.

It is noted that for open microstrip structures, closed form asymptotic Green's functions have been developed in [11]–[13]. In this paper, we use the complex image method of [1] to derive closed form spatial Green's functions for shielded microstrip structures.

In the following sections, the homogeneous dielectric problem of Fig. 1(a) is discussed first to show the techniques used in this paper. Then these techniques are applied to solve the layered dielectric problem of Fig. 1(b). It will be evident that the same techniques are also applicable to obtain the closed form vector and scalar potentials for an electric dipole in multiple dielectric layers between two ground planes.

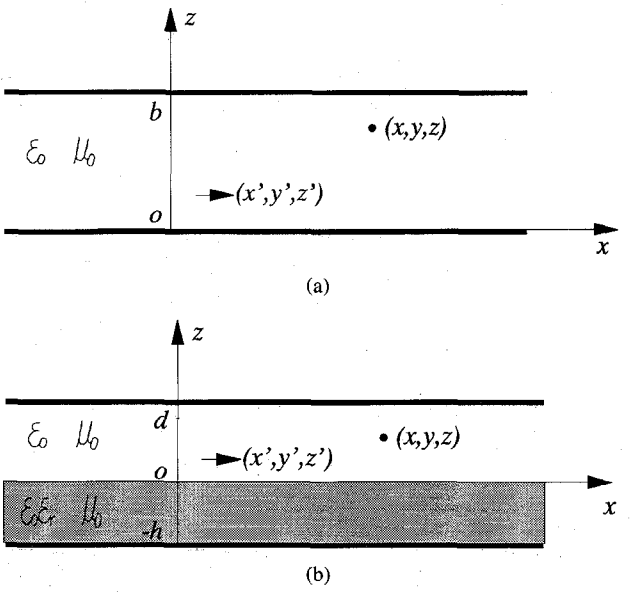

Fig. 1. (a) Horizontal electric dipole located between two ground planes. (b) Horizontal electric dipole located in a top-covered microstrip substrate.

II. Homogeneous Dielectric Between Two Ground Planes

Fig. 1(a) shows an x-directed electric dipole located in the air region bounded by two ground planes. Using the integral transformation technique [2], the vector and scalar potential Green's functions in spatial domain can be represented in the following integral form:

$$\frac{4\pi}{\mu_0} G_A^{xx} = 4\pi\epsilon_0 G_q = \int_{-\infty}^{\infty} \frac{1}{j2k_{z0}} T_{\mathrm{TE}} \cdot H_0^{(2)}(k_\rho \rho) k_\rho \, dk_\rho \qquad (1)$$

where

$$T_{\mathrm{TE}} = \frac{(1 - e^{-j2k_{z0}z'})(1 - e^{-j2k_{z0}(b-z)})e^{-jk_{z0}(z-z')}}{1 - e^{-j2k_{z0}b}}, \qquad \text{for } z \geq z'$$

$$k_{z0}^2 = k_0^2 - k_\rho^2, \quad k_0^2 = \omega^2 \mu_0 \epsilon_0. \qquad (2)$$

T_{TE} is the transmission coefficient of TE_z (i.e., with $H_z = 0$, also known as LSM [2]) plane wave spectrum from source plane ($z = z'$) to field plane ($z = z$). It can be easily derived using a wave matrix technique similar to [2], [7]. By exchanging the locations of z and z', the expression (2) is also applicable for $z \leq z'$.

To obtain an *image* expansion from (1), we expand T_{TE} into Taylor series, i.e.,

$$T_{\mathrm{TE}} = \sum_{n=0}^{\infty} \{\exp[-jk_{z0}(2nb + z - z')] - \exp[-jk_{z0} \cdot (2nb + z + z')] - \exp[-jk_{z0}[2(n+1)b - z - z'] + [\exp - jk_{z0}[2(n+1)b - z + z']]\}. \qquad (3)$$

Substituting (3) into (1), and using the Sommerfeld Identity [8], the spectral integral (1) can be put into the following series form:

$$\frac{4\pi}{\mu_0} G_A^{xx} = 4\pi\epsilon_0 G_q = \sum_{n=0}^{\infty} \left[\frac{e^{-jkor_{n1}}}{r_{n1}} - \frac{e^{-jkor_{n2}}}{r_{n2}} - \frac{e^{-jkor_{n3}}}{r_{n3}} + \frac{e^{-jkor_{n4}}}{r_{n4}} \right] \qquad (4)$$

where

$$r_{n1} = \sqrt{\rho^2 + (2nb + z - z')^2}, \quad r_{n2} = \sqrt{\rho^2 + (2nb + z + z')^2}$$
$$r_{n3} = \sqrt{\rho^2 + [2(n+1)b - z - z']^2},$$
$$r_{n4} = \sqrt{\rho^2 + [2(n+1)b - z + z']^2}.$$

Obviously expression (4) stands for a summation of an infinite number of images of the dipole due to the upper and lower ground planes.

To obtain a *modal* expansion from (1), we rewrite T_{TE} of (2) in the following form:

$$\frac{1}{j2k_{z0}} T_{\mathrm{TE}} = \frac{1}{2k_{z0}} tg\left(\frac{k_{z0}b}{2}\right) \frac{\sin(k_{z0}z')\sin(k_{z0}(b-z))}{\sin^2(k_{z0}b/2)}. \quad (5)$$

It is noticed that the function at the right hand side of (5) is *even* with respect to k_{z0}, which implies that there are no branch points on the complex k_ρ plane. In other words, the function at the right hand side of (5) is a *meromophic function* on the complex k_ρ plane. Physically, this feature corresponds to the fact that there is no radiation into infinity in the stripline circuits, since all the energy is restricted between the upper and lower ground planes. Using the Mittag-Leffler theorem for the tangent factor [9], expression (5) can be expanded into the following series:

$$\frac{1}{j2k_{z0}} T_{\mathrm{TE}} = \frac{2}{b} \sum_{\substack{n=1 \\ n=\text{odd}}}^{\infty} \frac{1}{k_\rho^2 - [k_0^2 - (n\pi/b)^2]} \cdot \frac{\sin(k_{z0}z')\sin(k_{z0}(b-z))}{\sin^2(k_{z0}b/2)}. \quad (6)$$

Substituting (6) into (1), and using the residue theorem [9] by enclosing all the singularities in the lower half of the complex k_ρ plane, the spectral integral (1) can be put into the following series form:

$$\frac{4\pi}{\mu_0} G_A^{xx} = 4\pi\epsilon_0 G_q = \frac{\pi}{jb} \sum_{\substack{n=1 \\ n=\text{odd}}}^{\infty} H_0^{(2)}(k_{\rho p}\rho) \cdot \sin\left(\frac{n\pi z'}{b}\right) \sin\left(\frac{n\pi(b-z)}{b}\right) \quad (7)$$

where

$$k_{\rho p}^2 = k_0^2 - (n\pi/b)^2$$

and $H_0^{(2)}(\cdot)$ stands for the second kind Hankel function of zero order. Obviously the expression (7) is a summation of an infinite number of modes excited by the dipole in a parallel plate waveguide. The terms with $k_0 > n\pi/b$ correspond to the propagating modes which decay with a distance dependence of $1/\sqrt{\rho}$. The terms with $k_0 < n\pi/b$ correspond to evanescent modes where the Hankel function of imaginary argument becomes a Kelvin function. If $b < \lambda_0/2$, i.e., $k_0 < \pi/b$, all the modes supported by the parallel plates are evanescent.

The modal expansion (7), which includes a finite number of propagating modes and an infinite number of evanescent modes, converges very slowly when the observation point is *close* (e.g., $<0.02\lambda_0$) to the dipole. On the other hand, the image expansion (4), which includes an infinite number of dipole images due to the two ground planes, converges very slowly when the observation point is *far* (e.g., $>0.2\lambda_0$) from the dipole. The convergence rates of these two expansions versus the field-to-source point distances have been studied in [3].

In the following, we use the complex image technique of [1] to derive a closed form expression, which *exploits the merits of both image and modal expansions* and converges rapidly over the whole range of the source-to-field point distances.

The term T_{TE} can be rewritten as follows:

$$T_{\mathrm{TE}} = e^{-jk_{z0}(z-z')} + (T_{\mathrm{TE}} - e^{-jk_{z0}(z-z')} - j2k_{z0}P_m) + j2k_{z0}P_m \quad (8)$$

where P_m is a truncated series of the right hand side of (6). The series is truncated such that only the propagating modes (i.e., real $k_{\rho p}$) are included in P_m. For instance, if $b < 0.5\lambda_0$, then $P_m = 0$; if $0.5\lambda_0 < b < \lambda_0$, then P_m is equal to only the first term of the series in (6).

T_{TE} is rewritten in this fashion for rapid convergence in the spatial domain, since the first and third terms have analytical inverse Hankel transforms. The second term of (8) can be approximated by a short exponential series using Prony's method [10]:

$$T_{\mathrm{TE}} - e^{-jk_{z0}(z-z')} - j2k_{z0}P_m = \sum_{i=1}^{N} a_i e^{-b_i k_{z0}}, \quad N \le 5 \quad (9)$$

where a_i and b_i are complex coefficients. For a chosen N, a_i and b_i are calculated for a given approximation path using Prony's method. The approximation path on the complex k_{z0} plane is given by a parametric equation, $k_{z0}/k_0 = -jt + (1 - t/T_0)$, $0 \le t \le T_0$, and has been discussed in [1]. Taking N in the range of $3 \sim 5$ yields an accuracy of better than 0.5% in calculating the spatial domain Green's function. Substituting (8), (9) into (1), we can put the spectral integral (1) into the following closed form:

$$\frac{4\pi}{\mu_0} G_A^{xx} = 4\pi\epsilon_0 G_q = G_0 + G_{ci} + G_{pm} \quad (10)$$

where

$$G_0 = \frac{e^{-jk_0 r_0}}{r_0}, \quad r_0 = \sqrt{\rho^2 + (z - z')^2} \quad (11)$$

$$G_{ci} = \sum_{i=1}^{N} a_i \frac{e^{-jk_0 r_i}}{r_i}, \quad r_i = \sqrt{\rho^2 + (-jb_i)^2} \quad (12)$$

$$G_{pm} = \frac{\pi}{jb} \sum_{\substack{n=1 \\ n=\text{odd}}}^{M} H_0^{(2)}(k_{\rho p}\rho) \cdot \sin\left(\frac{n\pi z'}{b}\right) \sin\left(\frac{n\pi(b-z)}{b}\right) \quad (13)$$

where G_0 is the source term due to the dipole itself, G_{ci} corresponds to the *complex image terms*, and G_{pm} corresponds to the *propagating mode* terms. It is noted in (11) and (12) that both the dipole and its complex images are located in a homogeneous free space, and represent an approximation of the *evanescent modes*. In other words, these dipole sources give the same near field as that given by an infinite number of evanescent modes. In (13), M is the number of modes extracted from the spectral integral (1). If $0 < b < \lambda_0/2$, then $M = 0$; if $\lambda_0/2 < b < \lambda_0$, then $M = 1$; and so on. For typical structures used in microwave stripline circuits, $(N + M)$ is no greater than $5 \sim 7$.

To show the accuracy of the complex image Green's function (10), an example of $b/\lambda_0 = 0.7$, $z = z' = 0.3\lambda_0$ is tested. In this example, only one LSM mode with $k_\rho/k_0 = 0.69985$ is extracted, and four complex images are used. The Green's functions calculated using closed form expression (10) and the exact image and modal expansions (4), (7) are plotted in Fig. 2. It is seen that the difference is indistinguishable, and generally $<0.5\%$.

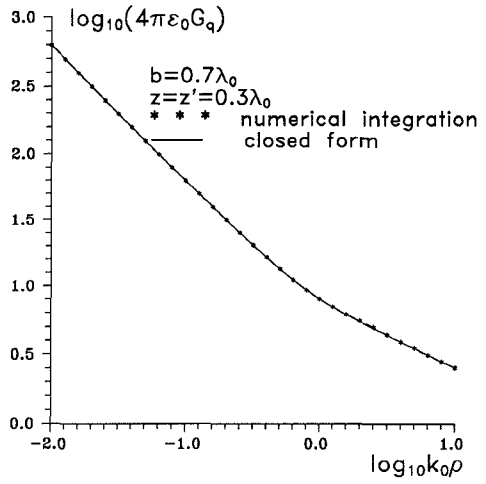

Fig. 2. Amplitude of $4\pi\epsilon_0 G_q$ for a homogeneous parallel plate structure of Fig. 1(a), where a pair of degenerate LSE and LSM modes are excited by the dipole.

III. Layered Dielectrics Between Two Ground Planes

As shown in Fig. 1(b), an x-directed electric dipole is located in air between the dielectric interface and the top ground plane. The spatial domain vector and scalar potentials in the air region can be represented in the following integral forms:

$$G_A^{xx} = \frac{\mu_0}{4\pi}\int_{-\infty}^{\infty} \frac{1}{j2k_{z0}} T_{\mathrm{TE}} \cdot H_0^{(2)}(k_\rho \rho) k_\rho \, dk_\rho \tag{14a}$$

$$G_q = \frac{1}{4\pi\epsilon_0}\int_{-\infty}^{\infty} \frac{1}{j2k_{z0}} T_q \cdot H_0^{(2)}(k_\rho \rho) k_\rho \, dk_\rho \tag{14b}$$

where

$$T_{\substack{\mathrm{TE}\\(\mathrm{TM})}} = \frac{[1 \mp e^{-j2k_{z0}(d-z)}]\,[1 \pm R_{\substack{\mathrm{TE}\\(\mathrm{TM})}} e^{-j2k_{z0}z'}]}{1 \pm R_{\substack{\mathrm{TE}\\(\mathrm{TM})}} e^{-j2k_{z0}d}} e^{-jk_{z0}(z-z')},$$

$$\text{for } z \geq z' \tag{15a}$$

$$T_q = T_{\mathrm{TE}} + \frac{k_{z0}^2}{k_\rho^2}\left(T_{\mathrm{TE}} + \frac{1}{jk_{z0}}\frac{\partial T_{\mathrm{TM}}}{\partial z}\right) \tag{15b}$$

where R_{TE} and R_{TM} are respectively TE_z and TM_z (also known as LSM and LSE, respectively [2]) wave reflection coefficients from the microstrip substrate. By exchanging the locations of z and z', the expressions in (15) are also applicable for $z \leq z'$. They can be derived by using the wave matrix technique [2], [7]:

$$R_{\mathrm{TE}} = -\frac{r_{10}^{\mathrm{TE}} + e^{-j2k_{z1}h}}{1 + r_{10}^{\mathrm{TE}} e^{-j2k_{z1}h}}, \quad R_{\mathrm{TM}} = -\frac{r_{10}^{\mathrm{TM}} - e^{-j2k_{z1}h}}{1 - r_{10}^{\mathrm{TM}} e^{-j2k_{z1}h}} \tag{16}$$

The reflection coefficients $r_{10}^{\mathrm{TE}} = (k_{z1} - k_{z0})/(k_{z1} + k_{z0})$ and $r_{10}^{\mathrm{TM}} = (k_{z0} - \epsilon_r k_{z0})/(k_{z1} + \epsilon_r k_{z0})$ are the same as those given in [1].

Although we can, in principle, get a modal expansion from (14) by finding all the eigenvalues (i.e., roots of the denominators of (15a)), the convergence of this modal expansion will be very slow for the near field calculation. On the other hand, an image expansion from (14) is very difficult due to the presence of dielectric interfaces. We here use the complex image technique of [1] to derive a closed form expression for the spectral integrals in (14). For conciseness, only G_q is examined below.

Similar to (8), we first rewrite T_q in (14b) as follows:

$$T_q = e^{-jk_{z0}(z-z')} + (T_q - e^{-jk_{z0}(z-z')} - j2k_{z0}P_m) + j2k_{z0}P_m \tag{17}$$

where in this case:

$$P_m = \sum_{p(\mathrm{TE\,and\,TM})} \frac{2k_{\rho p} Res_q}{k_\rho^2 - k_{\rho p}^2}, \quad Res_q = \lim_{k_\rho \to k_{\rho p}} (k_\rho - k_{\rho p}) \cdot T_q \tag{18}$$

where $k_{\rho p}$ stands for a pole on the real axis of complex k_ρ plane. The poles located in $[0, k_0]$ correspond to the waveguide modes of both LSE and LSM types trapped by the top and bottom ground planes, and the poles in $[k_0, \sqrt{\epsilon_r}k_0]$ correspond to the surface wave modes of both LSE and LSM types trapped by the dielectric slab. The poles located on the imaginary axis of complex k_ρ plane are not extracted from the spectral function T_q. Their contributions to the spectral integral will be included in the complex images discussed below.

Similar to (8), it is noted in (17) that only the source term $e^{-jk_{z0}(z-z')}$ and the propagating mode terms $j2k_{z0}P_m$ are extracted from the spectral function T_q. This is different from [1] where some nearby (and therefore strong) quasi-dynamic images were extracted as well. Due the presence of top and bottom ground planes, the quasi-dynamic images, derived under the approximation condition $k_{z0} \approx k_{z1}$ [1], [6], have the form of a double summation which converges slowly. For this reason, we now approximate all the remaining terms $(T_q - e^{-jk_{z0}(z-z')} - j2k_{z0}P_m)$ by a short exponential series of complex images similar to (9), using Prony's method. From the Sommerfeld identity and the residue theorem, the following closed form expression for G_q is obtained:

$$4\pi\epsilon_0 G_q = G_0 + G_{q,ci} + G_{q,pm} \tag{19}$$

where

$$G_0 = \frac{e^{-jk_0 r_0}}{r_0}, \quad r_0 = \sqrt{\rho^2 + (z-z')^2} \tag{20}$$

$$G_{q,ci} = \sum_{i=1}^{N} a_i \frac{e^{-jk_0 r_i}}{r_i}, \quad r_i = \sqrt{\rho^2 + (-jb_i)^2} \tag{21}$$

$$G_{q,pm} = \frac{1}{4\pi\epsilon_0}(-2\pi j) \sum_{p(\mathrm{TE\,and\,TM})} Res_q H_0^{(2)}(k_{\rho p}\rho) k_{\rho p}. \tag{22}$$

It is seen in (19) that the closed Green's function is composed of a source term G_0, N complex image terms and the possible propagating mode terms of LSE and LSM types. For typical structures used in microwave integrated circuits, the total number of terms in (19) is no greater than 10.

A similar closed form expression for G_A^{xx} can also be obtained by processing the spectral function T_{TE} in the same manner as T_q. The final solution is given below:

$$\frac{4\pi}{\mu_0} G_A^{xx} = G_0 + G_{A,ci}^{xx} + G_{A,pm}^{xx} \tag{23}$$

where $G_{A,ci}^{xx}$ has the same form as (21) except for different coefficients a_i and b_i, and $G_{A,pm}^{xx}$ has the same form as (22) except that only the propagating modes of TE_z (i.e., LSM) type are involved in $G_{A,pm}^{xx}$.

To show the accuracy of the complex image Green's functions (19) (23), a shielded microstrip substrate with $\epsilon_r = 12.6$, $h/\lambda_0 = 0.1$, $d/\lambda_0 = 0.6$ (see Fig. 1(b)) is tested. In this example, three LSE modes and two LSM modes are excited by the dipole. The

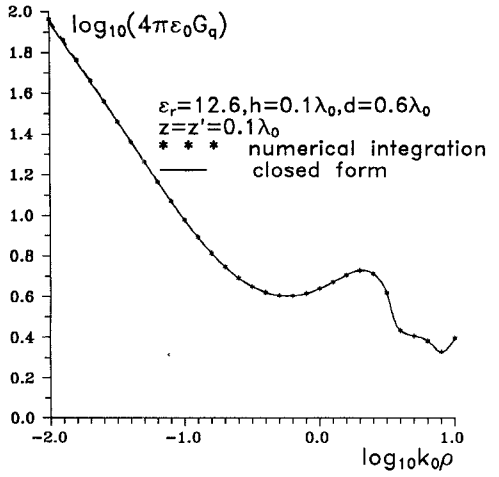

Fig. 3. Amplitude of $4\pi\epsilon_0 G_q$ for a top-covered microstrip structure of Fig. 1(b), where three LSE modes and two LSM modes are excited by the dipole.

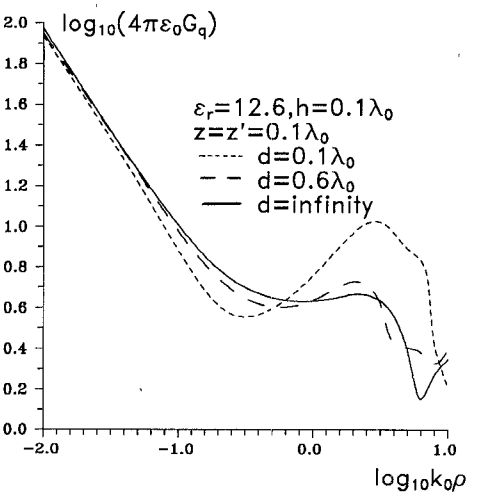

Fig. 4. Effect of top cover on the microstrip Green's function.

Green's function $4\pi\epsilon_0 G_q$ calculated using closed form expression (19) and the numerical integration of (14b) is plotted in Fig. 3. It is seen that the difference is indistinguishable, and generally $<0.5\%$. It is also noted in Fig. 3 that the amplitude of the Green's function $4\pi\epsilon_0 G_q$ starts to oscillate when the field-to-source distance is greater than a certain value (i.e., $\log_{10} k_0\rho > -0.5$). This oscillation is due to the interference of the five propagating modes existing in the structure.

To indicate the effect of top metallic cover on the microstrip Green's function, Fig. 4 compares the amplitudes of $4\pi\epsilon_0 G_q$ for an open microstrip substrate of [1] and the top-covered microstrip substrate of Fig. 2(b) with different plate heights. It is seen that when the top plate gets close to the substrate surface (e.g., $d = h = 0.1\lambda_0$), the Green's function is significantly disturbed.

IV. Discussions and Conclusion

Although the modal solution and the more general spectral integral solution are available for the problems of dipole radiation in homogeneous or layered dielectrics between two ground planes, they are usually time-consuming in numerical calculation. This paper presents a numerically efficient technique to obtain the closed form vector and scalar potentials for this type of problems. It has been shown that the closed form expression of this paper usually consists of no more than ten terms, each term standing for either a complex image or a propagating mode. As long as the complex image coefficients a_i and b_i are obtained, the closed form expression can be used for calculating the potential at any point in the concerned region.

It is noticed that the complex image coefficients a_i and b_i in (12) and (21) are dependent on the source and field locations z and z'. It fact we could also make the approximated spectral function independent of z and z', as done in [1]. This is at the expense of extra analytical manipulation as well as an increased number of image terms in the closed form expression. In practical MMIC circuits, metallizations may have finite thickness or may be located in different dielectric layers. Therefore several sets of complex image coefficients may be needed to represent different heights z and z' of the source and field locations.

In obtaining the complex image coefficients, an Nth order polynomial equation and two $N \times N$ matrix equations are to be solved in Prony's method [10], where N (usually ≤ 5) is the number of images. This process takes little time on a personal computer. In implementing Prony's method, similar to [1], the truncation point T_0 and the number of images N have to be set *a priori*. The truncation point of the approximation path should be chosen far enough from the origin of complex k_{z0} plane so that sufficient spectral information is provided to generate the complex images. For instance, in the situation of $z = z'$ the spectral function T_q approaches to a constant when $k_\rho \to \infty$. This constant corresponds to an image which coincides with the source dipole. Therefore the truncation point must be chosen such that at least two points are sampled near the constant region to recover this image term. The accuracy of the Green's function approximation is sensitive to the number of images N. Taking N in the range of $3 \sim 5$ is typical to obtain an accuracy of 0.5%. A larger number N does not give any better results, and sometimes may cause the results to diverge.

It is the choice of N and T_0, not the intermediate steps of the complex image coefficients, that ultimately affect the accuracy of the Green's function. Therefore as long as one follows the Prony's method procedure given in [10], one need not worry about the accuracy of the complex image coefficients a_i and b_i.

Although only a shielded microstrip substrate is examined as a layered dielectric example, the method of this paper is equally applicable to the structures with multiple dielectric layers between two ground planes.

References

[1] Y. L. Chow, J. J. Yang, D. G. Fang, and G. E. Howard, "A closed form spatial Green's function for the thick microstrip substrate," *IEEE Trans. Microwave Theory Tech.*, vol. 39, no. 3, pp. 588–592, Mar. 1991.

[2] R. E. Collin, *Field Theory of Guided Waves*. 2nd ed. New York: McGraw-Hill, 1991, pp. 78–87, pp. 184–192, pp. 412–416.

[3] D. A. Huber and Y. L. Chow, "The 3-D Green's function and the moment method for stripline circuits," in *1990 IEEE AP-S Symp., Dig.*, Dallas, TX, May 7–11, pp. 312–315.

[4] I. Tai Lu and R. L. Olesen, "Analysis of transmission line structures using a new image-mode Green's function," *IEEE Trans. Microwave Theory Tech.*, vol. 38, no. 6, pp. 782–785, June, 1990.

[5] N. K. Das and D. M. Pozar, "Generalized spectral domain Green's function for multilayer dielectric substrates with application to multilayer transmission lines," *IEEE Trans. Microwave Theory Tech.*, vol. MTT-35, pp. 326–335, Mar., 1987.

[6] J. R. Mosig and T. K. Sarkar, "Comparison of quasi-static and exact electromagnetic fields from a horizontal electric dipole above a lossy dielectric backed by an imperfect ground plane," *IEEE Trans. Microwave Theory Tech.*, vol MTT-34, no. 4, pp. 379-387, Apr. 1986.
[7] J. A. Kong, *Theory of Electromagnetic Waves*. New York: Wiley, 1986, ch. 3.
[8] J. A. Stratton, *Electromagnetic Theory*. New York: McGraw-Hill, 1941, pp. 576, Eq (17).
[9] J. Duncan, *The Elements of Complex Analysis*. New York: Wiley, 1968. pp. 214-220.
[10] R. W. Hamming, *Numerical Methods for Scientists and Engineers*. New York: Dover, 1973, pp. 620-622.
[11] M. Marin, S. Barkeshli, and P. H. Pathak, "Efficient analysis of planar microstrip geometries using a closed-form asymptotic representation of the grounded dielectric slab Green's function," *IEEE Trans. Microwave Theory Tech.*, vol 37, no. 4, pp. 669-679, Apr. 1989.
[12] S. Barkeshli, P. H. Pathak, and M Marin, "An asymptotic closed form microstrip surface Green's function for the efficient moment method analysis of mutual coupling in microstrip antennas," *IEEE Trans. Antennas Propagat.*, vol. 38, no. 9, Sept. 1990, pp. 1374-1383.
[13] ——, "Closed form asymptotic representations for the grounded planar single and double layer material slab Green's functions and their applications in the efficient analysis of arbitrary microstrip geometries," presented at the *Int. Conf. on Directions in Electromagnetic Wave Modeling*, New York, Oct. 1990.

Comparison of Measured and Simulated Data in an Annular Phased Array Using an Inhomogeneous Phantom

Dennis M. Sullivan, Dale Buechler, and Frederic A. Gibbs

Abstract—**Computer simulation is being used to plan patient treatments for deep regional hyperthermia in the Sigma 60 applicator of the BSD-2000 Hyperthermia System. The method used is the finite-difference time-domain (FDTD) method. Like all simulation methods, confirmation of the accuracy via measured data is important. Until now, most such measurements in the Sigma 60 were done with homogeneous phantoms. A new phantom using both muscle and fat equivalent material has been constructed, presenting a more challenging simulation problem to the FDTD method. The description of the phantom and the results of comparisons between simulated and measured data are presented.**

I. Introduction

In deep regional hyperthermia cancer therapy, one of the most widely used devices is the Sigma 60 applicator of the BSD-2000 Hyperthermia System (BSD Medical, Salt Lake City, UT). This employs eight dipole antennas positioned around a 60 cm annulus, a configuration known as an annular phased array (APA). The eight dipoles are arranged in four groups of two each, referred to as quadrants. Although the four quadrants are all driven at the same frequency (the frequency range is 60 to 120 MHz), the amplitude and phase on each quadrant can be set independently. This ability to independently set the amplitudes and phases, as well as the selection of the frequency, presents a wide range of input parameters which has motivated the use of computer simulation for treatment planning in the Sigma 60 [1]–[3].

Recently, the implementation of a clinical treatment planning program using the finite-difference time-domain (FDTD) method has been described [4]. The accuracy of this method was tested by comparison of measurements made in a homogeneous phantom. In this paper, further verification will be presented with temperature measurements in an inhomogeneous phantom, which we will refer to as the Utah phantom.

Manuscript received May 31, 1991; revised September 21, 1991. This work was supported by grants CA 29578 and CA 44665 from the National Cancer Institute.

D. M. Sullivan is with the Department of Radiation Oncology, Stanford University School of Medicine, Stanford, CA 94305.

D. Buechler and F. A. Gibbs are with the Division of Radiation Oncology, University of Utah School of Medicine, Salt Lake City, UT 84132.

IEEE Log Number 9105445.

II. Phantom Construction

The Utah phantom used is a CDRH [5] elliptical phantom filled with two materials, one to simulate muscle and one to simulate fat or bone (Fig. 1). The muscle material was constructed from a recipe by Guy [6], with a slight variation: only 75% as much salt was used, giving a material with estimated relative dielectric constant of 60 and conductivity of 0.58 S/m. The fat material was constructed from a recipe by Lagendijk and Nilsson [7], giving a material with a relative dielectric constant of about 8 and a conductivity of about 0.05 S/m.

The phantom was constructed to roughly simulate the lower abdomen and pelvis, although the intent of its design was more that of a buildable inhomogeneous structure than an anatomic simulation. Thirteen catheters were placed in such a way that temperature measurements could be made at enough points to be representative of the SAR pattern within the phantom. The catheters were 16 gauge, large enough to allow easy movement of the temperature probes of the BSD-2000 [8].

III. Experimental Procedure

The energy deposition pattern throughout the phantom was determined by measuring the temperature increase at various points after power was applied for a short period of time in the Sigma 60 applicator. Using three temperature probes at a time, the probes were pushed all the way to the ends of the catheters. The automatic mapping feature of the BSD-2000 was used to move the probes in 1 cm increments, waiting 4 seconds for the temperature measurement to reach equilibrium, and recording it before moving on to the next position. One such reading was made before applying power and another was made after applying 1000 W for 2 min. The temperature difference was then calculated. These temperature differences were compared to the SAR patterns predicted by the FDTD simulation.

To do the FDTD simulation, a model of the phantom was simulated by assigning the corresponding properties of fat or muscle to the 1 cm cells which make up the 3-dimensional model. (This is similar to the way patient models are created for clinical simulations [9].) Approximately 30 000 cells were required for this phantom. The 3-D problem space used to simulate the phantom and the Sigma 60 was $74 \times 74 \times 68 = 372\,368$ cells. This required 10 megawords of core memory and 200 CPU seconds on a Cray YMP supercompter to simulate. Four such runs, corresponding to the four quadrants were necessary to obtain the complex E field at every point in the phantom; the SAR's were determined from these complex E fields. (This is described in detail in [4].)